quantum reports

MDPI

Article

An Overview of Basis Set Effects for Diatomic Boron Nitride Compounds ($B_2N^{(\mp,0)}$): A Quantum Symmetry Breaking

Majid Monajjemi [1,*], Fatemeh Mollaamin [2] and Neda Samiei Soofi [3]

[1] Department of Chemical Engineering, Central Tehran Branch, Islamic Azad University, Tehran 1496969191, Iran
[2] Department of Biomedical Engineering, Faculty of Engineering and Architecture, Kastamonu University, Kastamonu P.O. Box 37150, Turkey
[3] Department of Chemistry, Science and Research Branch, Islamic Azad University, Tehran 1477893855, Iran
* Correspondence: maj.monajjemi@iauctb.ac.ir

Abstract: The symmetry breaking (SB) of $B_2N^{(-,0,+)}$ not only exhibits an energy barrier for ionic or neutral forms dependent on various basis sets but it also exhibits a few SBs due to the asymmetry stretching and bending mode interactions. SB obeys the mechanical quantum theorem among discrete symmetries and their connection to the spin statistics in physical sciences. In this investigation, the unusual amount of energy barrier of SBs appeared upon the orbit–orbit coupling of BNB (both radical and ions) between transition states and the ground state. Our goal in this study is to understand the difference among the electromagnetic structures of the ($B_2N^{(\mp,0)}$) variants due to effects of various basis sets and methods and also the quantum symmetry breaking phenomenon. In the $D_{\infty h}$ point group of ($B_2N^{(\mp,0)}$) variants, the unpaired electron is delocalized, while in the asymmetric $C_{\infty v}$ point group, it is localized on either one of the B atoms. Structures with broken symmetry, $C_{\infty v}$, can be stable by interacting with the $D_{\infty h}$ point group. In viewpoints of quantum chemistry, the second-order Jahn–Teller effect permits the unpaired electron to localize on boron atom, rather than being delocalized. In this study, we observed that the energy barrier of SB for BNB increases by post HF methods.

Keywords: boron nitride cages; hyperfine properties; dipole moment; Chelp G; EPR-II; EPR-III; MESP (EP)

Citation: Monajjemi, M.; Mollaamin, F.; Samiei Soofi, N. An Overview of Basis Set Effects for Diatomic Boron Nitride Compounds ($B_2N^{(\mp,0)}$): A Quantum Symmetry Breaking. *Quantum Rep.* **2022**, *4*, 338–350. https://doi.org/10.3390/quantum4030024

Academic Editors: Jorge Garza, Rubicelia Vargas and Andrei L. Tchougréeff

Received: 14 July 2022
Accepted: 1 September 2022
Published: 8 September 2022

1. Introduction

1.1. BNB Structures

A deep study on $B_x N_{3-x}$ (x = 1, 2) was accomplished by Martin et al. on BNB structures using theoretical methods and spectroscopic measurements [1]. The UHF/6-311G (p, d) level of calculation exhibited an asymmetric linear combination of $B_2N^{(0)}$ in its ground state, and it contains a low bending frequency of 72 cm^{-1} [1,2]. $B_2N^{(-)}$, $B_2N^{(+)}$ and $B_2N^{(0)}$ compounds have been studied as the most complicated cases of symmetry breaking (SB), and they are both real and sometimes artifactual due to the pseudo-second-order Jahn–Teller effect. Although several experimental or theoretical discussions have been performed for these subjects of studies [1–5], there are no any quantum reports of SB for ionic structures resulting from the calculation of various basis sets [6–12]. In total, all scientists agreed with the linearity of these compounds but only in its ground state, such as ($\widetilde{X}^2\Sigma_u^+$) and ($\widetilde{X}^1\Sigma_g^+$) in its radical or ionic forms, respectively. Paldus [9,10] investigated the electronic structure of $B_2N^{(0)}$ using multi-reference coupled cluster optimizations, including both singlet and doublet states with the RMR CCSD (T) Hamiltonian using cc-pVDZ, cc-pVTZ and (cc-pVQZ). In other approaches CCSD (T), BD (T) and the RMR CCSD (T) methods also exhibited an asymmetric configuration of unequal BN bound lengths with low barrier energy [1,3]. The $B_2N^{(0)}$ structure has been confirmed by Raman spectroscopy [4], which can also be synthesized

according to the $B(^2P) + N(^4S) \rightarrow BN(^1\Sigma^+)$ and $B(^2P) + BN(^1\Sigma^+) \rightarrow BNB(^2\Sigma^+_{(u)})$ reactions [12–16]. In addition, the state of $\widetilde{A}^2\Sigma^+_g(B_2N^-)$ was recognized using photoelectron spectroscopic studies (PES) at 6335 ± 20 cm^{-1} above the $\widetilde{X}^2\Sigma^+_u$ (ground state) [2]. Asmis [2] predicted where the spectrum in the 350 and 265 nm photoelectron analysis of B_2 N^- indicates a ground state with an electronic configuration as $(\widetilde{X}^1\Sigma^+_g)$. He also demonstrated the position of excited-state $B_2N^{(0)}$ $(\widetilde{X}^2\Sigma^+_u)$ and $(\widetilde{A}^2\Sigma^+_g)$ with a linear symmetry combination as transition reactions as follows: $\widetilde{X}^1\Sigma^+_g \rightarrow \widetilde{X}^2\Sigma^+_u + e^-$ and $\widetilde{X}^1\Sigma^+_g \rightarrow \widetilde{A}^2\Sigma^+_g + e^-$. Moreover, IR spectroscopy also observed a spectrum at 6001 cm^{-1} due to the $\widetilde{A}^2\Sigma^+_g \rightarrow \widetilde{X}^2\Sigma^+_u$ reaction [7,8]. Walsh [17] showed that an ion with 15 or less valence ($nS + nP$) electrons would be linear, while up to 20 valence electrons would cause it to bend; thus, they would become stronger in bending structures if the number of valence electrons increased. Walsh's idea properly interpreted all $BN^{(-,0,+)}$ variant behaviors due to the eleven valence electrons in the ground electronic configuration from $(\widetilde{X}^2\Sigma^+_u)$ to $(\widetilde{X}^1\Sigma^+_g)$ for B_2N $^{(0)}$ and B_2N^-, respectively.

1.2. Quantum Theory of Symmetry Breaking (SB)

SB obeys the quantum mechanics theorem among the discrete symmetries and their connection to spin statistics for physical sciences. The related wave function can belong to any representation of the character tables in the group theory, whether degenerate or not. According to the Pauli Exclusion Principle, a fermion belongs to an antisymmetric irreducible representation of the associated symmetric group. Therefore, the wave function of any state should satisfy two eigenvalues: first, the Schrödinger equation and, second, $P|\psi\rangle = (-1)^P|\psi\rangle$, which is any permutation of the symmetric group S_N that can be assumbed as a constraint wave function and should satisfy the Schrödinger equation. Wigner [18] interpreted that the exact electronic wave function satisfying the Pauli principle that is simultaneously an eigenfunction of S^2 and S_Z should be written as follows:

$$\psi_{S,M}\left(\vec{x_1}, \vec{x_2}, \ldots \vec{x_N}\right) = \left(\sqrt{f_N^S}\right)^{-1} \Sigma_{i=1}^{f_N^S} \Phi_i\left(\vec{r_1}, \vec{r_2}, \ldots \vec{r_N}\right) \Theta_i(\sigma_1, \sigma_1, \ldots \sigma_N)$$

where Φ_i is the spinless Schrödinger equation, and Θ_i includes spin eigenfunctions, and both belong to dual representations of the symmetric group; moreover, f_N^S is the number of spin eigenfunctions. It is obvious that a trial wave function might be presented by the Wigner theorem [18]. By considering a zero wave function as ${\psi_{S,M}}^0$ that also satisfies the Pauli principle, the following can be described:

$${\psi^0}_{S,M} = \Sigma_{K=1}^{f_N^S} C_k^s \, {\psi^0}_{S,M;k},$$

where

$$\begin{gathered} {\psi^0}_{S,M;k} = (N!)^{0.5} A\left(\Phi_0^N \Theta_{S,M;k}\right) = \\ (N!)^{-0.5} \Sigma_p (-1)^P \left(P^r \Phi_0^N\right)\left(P^\sigma \Theta_{S,M;k}\right) = \\ (N!)^{-0.5} \Sigma_p (-1)^P \left(P^r \Phi_0^N\right) \Sigma_{l=1}^{f_N^S} U_{lk}^s(P) \Theta_{S,M;l} = \\ \sqrt{f_N^S} \Sigma_{l=1}^{f_N^S} \Theta_{S,M;l} \left(\frac{f_N^S}{N!}\right)^{0.5} \times \Sigma_p (-1)^P U_{lk}^s(P) \left(P^r \Phi_0^N\right) \end{gathered}$$

Here, $A = (N!)^{-0.5} \Sigma_p (-1)^P P$ and $P = P^r P^\sigma$, and $U^S(P)$ denotes the antisymmetric representation of the symmetric group generated by spin functions $\Theta_{S,M;k}$ $k = 1, 2, \ldots$ f_N^S. If the trial wave function cannot be replaced in the above formula, the electrons will not be treated as indistinguishable particles. Since there are f_N^S spin functions that span the full space of the irreducible representations of the symmetric group, we should consider all of them. The symmetry breaking (SB) problem is related to a lack of the "correct" permutation symmetry of the wave function adopted to solve the problem, and it is by no means a real effect. Within the subject of quantum theory, the term "spatial symmetry breaking" can be interpreted in two ways: The first is the lack of a broken wave function for transformations

as an irreducible representation of the related point group and the second is a preference of the nuclear framework for a lower-symmetry geometry. The first item is due to the approximate wave function or artifactual in the proper wave functions. Relaxed symmetry constraints for obtaining lower-energy but symmetry0contaminated wave functions were described by Lowdin [19] as the symmetry dilemma. The second item is related to the real or artifactual wave function and symmetry breaking in the nuclear framework due to first-order Jahn–Teller effects.

2. Materials and Methods

Various Basis Sets

EPR-III and EPR-II basis sets of Baron [20] exhibit the most applicable results for electrostatic potential fitting (ESP). EPR-II is a double-ζ basis set with a single set of polarization functions for B to F [21,22] that is useful for $B_2N^{(\mp,0)}$ calculations. EPR-III is also a triple-ζ consisting of diffuse functions, d-polarizations, and a set of normal polarization functions, while compared with EPR-II, the s-part improved for better optimization in a set of B to F atoms [20–24]. In other words, the active space of the CASSCF can be considered, and all valence electrons and orbitals of these atoms can be considered for any further calculations with the post-HF method, including 11 active electrons and 12 active orbitals for $B_2N^{(0)}$ and 10 and 12 electrons for $B_2N^{(+)}$ and $B_2N^{(-)}$, respectively. Due to our target for comparison, which includes various basis sets and their effects on the symmetry breaking of artifactual or trial wave functions, $B_2N^{(\mp,0)}$ has been optimized using several levels of the theory, such as CASSCF (11, 12)/cc-PVQZ for $B_2N^{(-)}$ and CASSCF (11, 12)/AUG-cc-PVQZ $B_2N^{(0)}$ and CASSCF (10, 12)/cc-PVQZ for $B_2N^{(+)}$. A spin orbit coupling constant has also been taken into account during CASSCF calculations [25,26]. The quadratic configuration interaction (CI) optimization containing single and double forms [27] has been also applied for evaluating various properties such as NBO, bonding analysis (AIM) [28], NPA or natural population analysis, electrostatic potentials and electrostatic potential-derived charges using the Merz–Kollman–Singh [29], chelp [30] or chelp G [31] methods. The hyperpolarizabilities have been measured via CISD, QCISD, MP_2 and CASSCF levels of optimization. The AIM software is applied for computing atomic charges, covalent bonds, localized orbitals and critical points to predict the atomic properties in $B_2N^{(\mp,0)}$ variants [28]. The representative atomic charges might be computed as average amounts over several states in $B_2N^{(\mp,0)}$. A detailed data of basis sets and the Hamiltonian related to the charge distribution can be found in Refs. [32–34]. ChelpG data can be computed using ab initio quantum chemical packages such as Gaussian or GAMESS-US [35] (Table 1).

Table 1. Contribution of various basis sets.

Basis Sets	Contraction Level	Contraction Scheme	N
6-311+G(3df)	Original	(12s6p3d1f)/[5s4p3d1f]	39
uC-6-311+G(3df)	Core-uncontracted	(12s6p3d1f)/[10s4p3d1f]	44
u-6-311+G(3df)	Fully uncontracted	(12s6p3d1f)/[12s6p3d1f]	52
aug-cc-pVTZ	Original	(11s6p3d2f)/[5s4p3d2f]	46
uC-aug-cc-pVTZ	Core-uncontracted	(11s6p3d2f)/[11s4p3d2f]	52
u-aug-cc-pVTZ	Fully uncontracted	(11s6p3d2f)/[11s6p3d2f]	58
aug-cc-pVQZ	Original	(13s7p4d3f2g)/[6s5p4d3f2g]	80
uC-aug-cc-pVQZ	Core-uncontracted	(13s7p4d3f2g)/[13s5p4d3f2g]	87
u-aug-cc-pVQZ	Fully uncontracted	(13s7p4d3f2g)/[13s7p4d3f2g]	93
aug-cc-pV5Z	Original	(15s9p5d4f3g2h)/[7s6p5d4f3g2h]	127
uC-aug-cc-pV5Z	Core-uncontracted	(15s9p5d4f3g2h)/[15s6p5d4f3g2h]	135
u-aug-cc-pV5Z	Fully uncontracted	(15s9p5d4f3g2h)/[15s9p5d4f3g2h]	144

Table 1. *Cont.*

Basis Sets	Contraction Level	Contraction Scheme	N
aug-cc-pV6Z	Original	(17s11p6d5f4g3h2i)/[8s7p6d5f4g3h2i]	189
uC-aug-cc-pV6Z	Core-uncontracted	(17s11p6d5f4g3h2i)/[17s7p6d5f4g3h2i]	198
u-aug-cc-pV6Z	Fully uncontracted	(17s11p6d5f4g3h2i)/[17s11p6d5f4g3h2i]	210
aug-cc-pCVTZ	Original	(13s8p4d2f)/[7s6p4d2f]	59
uC-aug-cc-pCVTZ	Core-uncontracted	(13s8p4d2f)/[13s6p4d2f]	65
u-aug-cc-pCVTZ	Fully uncontracted	(13s8p4d2f)/[13s8p4d2f]	71
aug-cc-pCVQZ	Original	(16s10p6d4f2g)/[9s8p6d4f2g]	109
uC-aug-cc-pCVQZ	Core-uncontracted	(16s10p6d4f2g)/[16s8p6d4f2g]	116
u-aug-cc-pCVQZ	Fully uncontracted	(16s10p6d4f2g)/[16s10p6d4f2g]	122

3. Results

Based on our previous study [36–52], $B_2N^{(0)}$ exhibits a linear structure in terms of ground state ($\widetilde{X}^2\Sigma_u^+$) where the electrons' occupancy are as follows: $1\sigma_g^2, 1\sigma_u^2, 2\sigma_g^2, 3\sigma_g^2, 2\sigma_u^2, 1\pi_u^4, 4\sigma_g^2$, and $3\sigma_u^1$. In addition, the electron configuration of the lowest excited state can be predicted as $\widetilde{A}^2\Sigma_{(g)}^+$, where its orbital occupancy can be exhibited as follows: $1\sigma_g^2$, $1\sigma_u^2$, $2\sigma_g^2, 3\sigma_g^2, 2\sigma_u^2, 1\pi_u^4, 4\sigma_g^1$, and $3\sigma_u^2$.

In addition, the $\widetilde{B}^2\Pi_g$ excited state can be written as $1\sigma_g^2$, $1\sigma_u^2, 2\sigma_g^2, 3\sigma_g^2, 2\sigma_u^2, \pi_u^4, 4\sigma_g^2, 1\pi_g^1$ (above the $\widetilde{A}^2\Sigma_g^+$), and it is subject to the Renner–Teller effect, and the further excited state depends on the $(^4\Pi_g)$ of triplet form. The electrostatic potential (EP) in ground and excited states of $B_2N^{(\mp,0)}$ and also the HOMO-LUMO gap, with isotropic Fermi contact couplings (MHz), are listed in Table 2. Our target of this study is to understand the difference between the electromagnetic structures of the $B_2N^{(\mp,0)}$ variants due to different basis sets and methods and also quantum symmetry breaking reports due to artifactual and trial wave functions. In the $D_{\infty h}$ point group of $B_2N^{(\mp,0)}$ variants, an unpaired electron is delocalized, while in the asymmetric $C_{\infty v}$ point group, it is localized on either one of the B atoms. Structures with broken symmetry, $C_{\infty v}$, can be stable by interaction to the $D_{\infty h}$ point group. In viewpoint of quantum chemistry, the second-order Jahn–Teller effect permits the unpaired electron to localize on the boron atom rather than being delocalized. The other two, which correspond to localizing the unpaired electron on one or both of the boron atoms, do not transform as an irreducible representation of the $D_{\infty h}$ symmetry for $B_2N^{(0)}$ radicals on N and either one of the B atoms (Table 2 and Figure 1a,b).

Table 2. Geometry optimization and electrical properties of $B_2N^{(-,0,+)}$ in ground and excited states.

State Number of Electron	E_e (*Hartree*) Isolated BNB	All Electron Configuration (Total Energy of $\|\alpha\rangle$ * (*Homo*−*Lumo*) **	β Electron Configuration Total Energy of $\|\beta\rangle$ * (*Homo*−*Lumo*) **	r_e (B_1N) r_e (NB_2)	A_1 (2,1,3,−2,−1) A_2 (2,1,3,−1,−2)
$\widetilde{X}^2\Sigma_u^+$ $(D_{\infty h})$	-104.078196 [b]	$[A']\pi_u^4, 4\sigma_g^2, 3\sigma_u^1\|\alpha\rangle = -0.4461$ [b] $* (-34.87079)$ [b] $** (-0.48614)$ [b]	$[B']$, $4\sigma_g^1\|\beta\rangle = -0.2620$ [b] $* (-34.15042)$ [b] $** (-0.17697)$ [b]	1.3198 [z] 1.3198 [z]	$A_1 = 180.0$ [z] $A_2 = 180.0$ [z]
$\widetilde{X}^2\Sigma^+$ $(C_{\infty v})$ (17e)	-104.078196 [a] -104.082033 [a′] -104.075492 [a″]	$[A], \pi^4, \sigma^2, \sigma^1\|\alpha\rangle = -0.44641$ [a] $* E(\|\alpha\rangle)(-34.87083)$ [a] $** (-0.48614)$ [a]	$[B]\sigma^1\|\beta\rangle = -0.26180$ [a] $* (-34.15046)$ [a] $** (-0.17697)$ [a]		

Table 2. *Cont.*

State Number of Electron	E_e (*Hartree*) Isolated BNB	All Electron Configuration (Total Energy of $\|\alpha\rangle$ * (*Homo*−*Lumo*) **	β Electron Configuration Total Energy of $\|\beta\rangle$ * (*Homo*−*Lumo*) **	r_e (B_1N) r_e (NB_2)	A_1 (2,1,3,−2,−1) A_2 (2,1,3,−1,−2)
$\widetilde{X}^2\Sigma_u^+$ ($D_{\infty h}$) (17e)	−103.639678	$[\boldsymbol{A'}]\pi_u^4, 4\sigma_g^2, 3\sigma_u^1\|\alpha\rangle = -0.42477$ [d] $*(-34.74888)$ [d] $**(-0.49245)$ [d]	$[\boldsymbol{B'}], 4\sigma_g^1\|\beta\rangle = -0.24844$ [d] $*(-34.06924)$ [d] $**(-0.18742)$ [d]	1.3176 [d] 1.3176 [d]	$A_1 = 180.0$ [d] $A_2 = 180.0$ [d]
$\widetilde{X}^2\Sigma_u^+$ ($D_{\infty h}$)	−104.159145 [f] −104.135552 [n]	$[\boldsymbol{A'}]\pi_u^4, 4\sigma_g^2, 3\sigma_u^1\|\alpha\rangle = -0.44701$ [f] $*(-34.86501)$ $**(-0.48249)$	$[\boldsymbol{B'}], 4\sigma_g^1\|\beta\rangle = -0.26341$ $*(-34.14329)$ $**(-0.17779)$	1.3275 [f] 1.3275	$A_1 = 180.0$ [f] $A_2 = 180.0$
$\widetilde{A}^2\Sigma_g^+$ (17e)	−104.104759 [k] −104.078173 [K']	$[\boldsymbol{A'}]\pi_u^4, 4\sigma_g^1, 3\sigma_u^2\|\alpha\rangle = -0.44638$ [u] $*(-34.8744)$ [u] $**(-0.48626)$ [u]	$[\boldsymbol{A'}]\pi_u^4, 4\sigma_u^1, = -0.26134$ $*(-34.15408)$ $**(-0.17666)$	1.3154 [k] 1.3154 [k]	$A_1 = 180.0$ [k] $A_2 = 180.0$ [k]
$\widetilde{B}^4\Pi_g$ (17e)	−104.029702 [h] −104.014117 [a]	$[\boldsymbol{A'}]\pi_u^4, \pi_g^2, \sigma_g^1\|\alpha\rangle = -0.26899$ [h] $*(-35.04484)$ [h] $*(-0.30125)$ [h]	$[\boldsymbol{A'}], \pi_u^2\|\beta\rangle = -0.4965$ [h] $*(-33.74801)$ $**(-0.50595)$	1.3079 [x] 1.3079 [x]	$A_1 = 180.0$ [x] $A_2 = 180.0$ [x]
$\widetilde{X}^1\Sigma_g^+$ (18e)	−104.196567 [a] −104.201914 [a'] −104.195017 [a'']	$[\boldsymbol{A'}]1\pi_u^4, 4\sigma_g^2, 3\sigma_u^2 = -0.13904$ [a] $*E(\|\alpha\rangle) = -32.48647$ [a] $**-0.36286$		1.335 [y] 1.335 [y]	$A_1 = 180.0$ [y] $A_2 = 180.0$ [y]
$\widetilde{X}^1\Sigma_g^+$ (18e)	−104.196566 [b]	$*E(\|\alpha\rangle) = -32.48644$ [b]		1.3291 [b] 1.3291	$A_1 = 180.0$ [b] $A_2 = 180.0$
$\widetilde{X}^1\Sigma_g^+$ (18e)	−104.114546 [c] −104.116282 [c'] −104.112568 [c'']	$[\boldsymbol{A'}]\pi_u^4, \sigma_g^2, \sigma_u^2 = -0.13454$ [c]		1.3459 [c] 1.3459 [c]	$A_1 = 179.8967$ [c] $A_2 = 179.9181$ [c]
$\widetilde{A}^3\Pi_u$ (18e)	−104.088466 [a] −104.116467 [h] −104.080948 [a'] −104.079253 [a'']	$[\boldsymbol{C}]\pi_u^4, 3\sigma_u^1, 1\pi_g^1\|\alpha\rangle =$ -0.03986 [h] $*E(\|\alpha\rangle) = -32.79721$ [h] $**-0.25941$ [h]	$[\boldsymbol{C'}]\pi_u^4, 4\sigma_g^1\|\beta\rangle =$ -0.01559 [h] $*E(\|\beta\rangle) = -32.26335$ [h] $**-0.14777$ [h]	1.3422 [w] 1.3422	$A_1 = 180.0$ [w] $A_2 = 180.0$ [w]
$\widetilde{B}^3\Sigma_g$ (16e)	−103.760922 [a] −103.776711 [h] −103.762855 [a'] −103.759058 [a'']	$\{[\boldsymbol{A'}]4\sigma_g^1, 3\sigma_u^1, \pi_u^4,\}$ [a] $\pi_u^2\|\alpha\rangle = -0.74323$ [a] $*E(\|\alpha\rangle)(-37.33372)$ [a] $**(-0.53385)$ [a]	$\{[\boldsymbol{A'}], \pi_u^2\|\beta\rangle = -0.75222\}$ [a] $*E(\|\beta\rangle)(-35.72475)$ [a] $**(-0.52131)$ [a]	1.2976 [w] 1.2976 [w]	$A_1 = 180.0$ [w] $A_2 = 180.0$ [w]
$\widetilde{X}^1\Sigma_g^+$ (16e)	−103.74543 [a] −103.805494 [a'] −103.754507 [a'']	$[\mathbf{D}](1\pi_u^4), (4\sigma_g^2 = -0.57788$ [a]) $*E(\|\alpha\rangle) = -36.52419$ [a] $**-0.17926$ [a]		1.2938 [v] 1.2938 [v]	$A_1 = 180.0$ [v] $A_2 = 180.0$ [v]
$\widetilde{X}^1\Sigma_g^+$ (16e)	−103.602313 [m] −103.301206 [g] −103.837742 [f] −103.790333 [h]	$[\mathbf{D}](1\pi_u^4), (4\sigma_g^2 = -0.57803$ [g]) $*E(\|\alpha\rangle) = -36.51985$ [g] $**-0.17944$ [g]		1.3156 [m] 1.3156 [m] 1.3003 [h] 1.3004 [h]	$A_1 = 179.981$ [m] $A_2 = 179.985$ [m]

* (Total Energy of $|\alpha\rangle$ or $|\beta\rangle$; ** *(Homo-Lumo).* (*a*) QCISD/EPR-III; (*d*) CASSCF(11,12)/UHF; (*z*) b3p86/6-31g*; (*a'*) MP_4D/EPR-III//QCISD/EPR-III; (*m*) CASSCF(10,12)/EPR-I (x) b3lyp/6-31g*; (*a''*) MP_4SDQ/EPR-III//QCISD/EPR-III; (*g*) CASSCF(10,12)rohfAUG-cc-pvqz; (*y*) m062x/epr-ii; (*b*) QCISD/EPR-III ([$\boldsymbol{A}$] : $1\sigma^2, 2\sigma^2, 3\sigma^2, 4\sigma^2, 5\sigma^2$: (*w*) b3lyp/6-31g*; (*c*) QCISD/EPR-II $[\boldsymbol{A'}] : 1\sigma_g^2, 1\sigma_u^2, 2\sigma_g^2, 3\sigma_g^2, 2\sigma_u^2$; (*v*) CASSCF(11,12)/AUG-cc-pvqz; (*c'*) MP_4D/EPR-II//QCISD/EPR-II: [$\boldsymbol{B}$] : $\sigma^1, \sigma^1, \sigma^1, \sigma^1, \sigma^1, \pi^2$; (*c''*) MP_4SDQ/EPR-II//QCISD/EPR-II; [$\boldsymbol{B'}$]: $1\sigma_g^1, 2\sigma_g^1, 1\sigma_u^1, 3\sigma_g^1, 2\sigma_u^1, 1\pi_u^2$; (*f*) CBS-lq; (*h*) QCISD(T)/EPR-III; [$\boldsymbol{C}$]: $1\sigma_g^2, 1\sigma_u^2, 2\sigma_g^2, 3\sigma_g^2, 2\sigma_u^2, 4\sigma_g^2$; (*n*) CBS4O; (*u*) TD/EPR-II; (*k*) TD/EPR-III//QCISD (T)/EPR-III; (*K'*) TD/EPR-III//QCISD/EPR-III; $[\boldsymbol{C'}] : 1\sigma_g, 1\sigma_u, 2\sigma_g, 3\sigma_g, 2\sigma_u$; [D]: $1\sigma_g^2, 2\sigma_g^2, 1\sigma_u^2, 3\sigma_g^2, 2\sigma_u^2$.

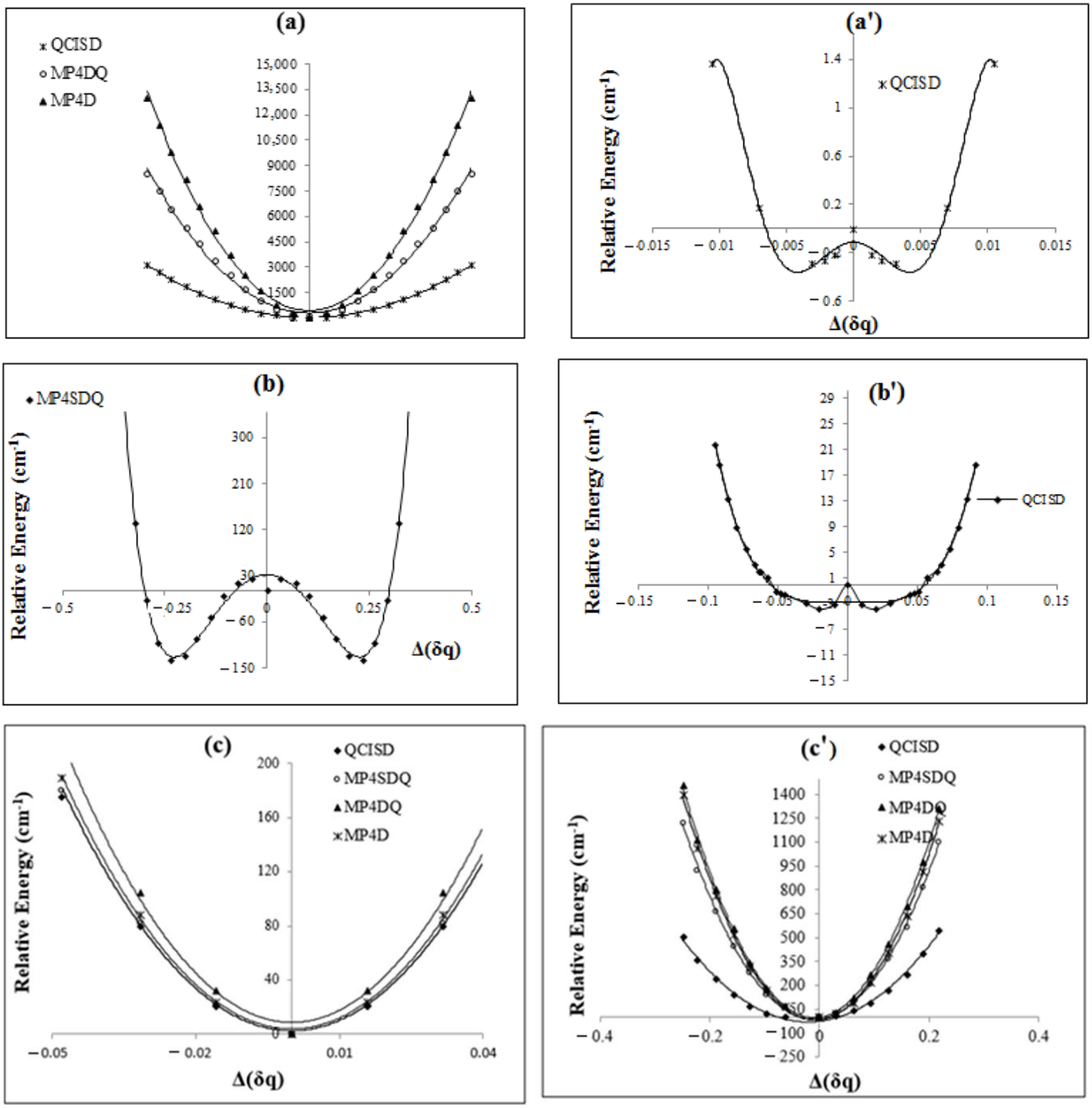

Figure 1. The $B_2N^{(-,0,+)}$ relative energies versus B-N-B bond distances at various levels of the theory: (**a**,**a′**) for cation, (**b**,**b′**) for radical and (**c**,**c′**) for anion.

The electrostatic potential (EP) in ground and excited states of $B_2N^{(\mp,0)}$ and also the HOMO-LUMO gap, with isotropic Fermi contact couplings (MHz), are listed in Table 2. Our target of this study is to understand the difference between the electromagnetic structures of the $B_2N^{(\mp,0)}$ variants due to different basis sets and methods and also the quantum symmetry breaking report due to artifactual and trial wave functions. In the $D_{\infty h}$ point group of $B_2N^{(\mp,0)}$ variants, the unpaired electron is delocalized, while in the asymmetric $C_{\infty v}$ point group, it is localized on either one of the B atoms. Structures with broken symmetry, $C_{\infty v}$, can be stable by interaction with the $D_{\infty h}$ point group. In viewpoint of quantum chemistry, the second-order Jahn–Teller effect permits the unpaired electron to

localize on the boron atom rather than being delocalized. The other two, which correspond to localizing the unpaired electron on one or both of the boron atoms, do not transform as an irreducible representation of $D_{\infty h}$ symmetry for the $B_2N^{(0)}$ radical on N and either one of the B atoms (Table 2 and Figure 1a,b). The unpaired electron of $B_2N^{(0)}$ in the $D_{\infty h}$ point group is delocalized. However, it is localized in the asymmetric $C_{\infty v}$ geometry for both radical and ion structures of $B_2N^{(\mp,0)}$ variants. On the other hand, there is a limitation for the unpaired electron of non-isolated BNB to obtain a delocalized state rather than being localized on a single boron atom between the two states of $D_{\infty h}$ and $C_{\infty v}$ symmetries.

These restrictions between localized and non-localized positions for unpaired electron result in an enhancement of the symmetry breaking effect of the $B_2N^{(\mp,0)}$ variants. Moreover, ESP charges, forces, $\gamma = (V_B - V_N)/r_{BN}$, attraction and repulsion energies (eV) of $B_2N^{(\mp,0)}$ variants in ground and excited states are listed in Table 3. The charges of MESP fitting for isolated BNB radicals and the summation of partial charges for two boron and one nitrogen ($B^{\delta q_1}$–$N^{\delta q_2}$–$B^{\delta q_3}$) in all items of the ranges from $\Delta = 0.0$ up to $\Delta = 0.07$ are zero (indicating a radical system) (Table 3). Interestingly, the summation of partial charges in $B^{\delta q_1}$–$N^{\delta q_2}$–$B^{\delta q_3}$ for $B_2N^{(0)}$ radical is not zero, and it changes according to the following: (0.23 + 0.23 + 0.52 = 0.98) for $\Delta^u = 0.0$, (0.24 + 0.23 + 0.52 = 0.99) for $\Delta^u = 0.02$ and so on (Table 3). The difference between Δ^u, Δ^k and Δ^x is due to various methods and basis sets that are applied; however, it is certain that the summation of partial charges in the $B_2N^{(0)}$ radical is far from zero and varies between 0.02 and 0.16. It can be due to the fact that the unpaired electron of nitrogen is localized while $B_2N^{(-)}$ is under the influence of the unpaired electron. It is obvious, for the excited state of radical forms, even though the change in MESP for both the excited state ($\widetilde{B}^4\Pi_g$) and ground state ($\widetilde{X}^2\Sigma_u^+$) is negligible, as opposed to the ground state (S = 1 of $B_2N^{(0)}$). Table 3 illustrates the charges from MESP fitting for isolated anions. The sum of partial charges (in $B^{\delta q_1}$–$N^{\delta q_2}$–$B^{\delta q_3}$) for all items from $\Delta = 0.0$ to $\Delta = 0.2$ is -1 (indicating an anion form); however, the total partial charges of $B^{\delta q_1}$–$N^{\delta q_2}$–$B^{\delta q_3}$ for $B_2N^{(-)}$ are not -1. It is due to the fact that the unpaired electron of nitrogen is localized. The parameters of "γ" for four bonds ($B_2 - N_1$, $B_3 - N_4$, $B_6 - N_5$ and $B_7 - N_8$) in Table 3 indicate that the stability sequences are as follows: $B_2N^{(-)} > B_2N^{(0))} > B_2N^{(+)}$. Using the Gaussian distribution of partial charges ranging from $\Delta^x = 0.0$ to $\Delta^x = 0.06$, the expectation values of charges were calculated, resulting in 0.21, 0.82 and 0.65 for the cation, anion and radical, respectively. The nitrogen of $B_2N^{(-,+,0)}$ is always positive for the radical and anion and negative for the cation, while in excited states, the sum of partial atomic charges is positive for all three forms. As observed in Figure 2, a cyclic radical or anion $B_2N^{(-,0)}$ in our calculations has not been observed; however, for the cation, there is a bulge in the curve at 90° in MP_4DQ and MP_4DSQ methods, which indicates a cyclic B_2N^+. At the SCF level, the lowest energy corresponds to a bent molecule with an angle of 90°; however, for the QCISD (T), MP_4DQ, MP_4DSQ, and HF/aug-cc-pVTZ calculations (Figure 2), the linear structure clearly has the lowest energies for radical and anion structures. In viewpoint of the wave function when the BNB has a $D_{\infty h}$ point group, the real wave function should convert as an irreducible representation of the $D_{\infty h}$ point group. However, "$4\sigma_g^2$" and "$3\sigma_u^1$" become close to degenerate when the two B–N bonds are asymmetrically stretched (while 6σ and 7σ MOs have the same symmetry). Thus, the excited state of $[core]6\sigma,7$, has a rather strong interaction with single and triple excitations. Anisotropic spin dipole coupling (MHZ), the differences of ($E_{acceptor_{(j)}} - E_{Donor_{(i)}}$) and NBO properties are listed in Table 4. It is obvious that the approximate electronic structure methods could suffer from an artifactual symmetry-breaking effect, which would, therefore, be challenged by a real Jahn–Teller distortion. The energy of these distortions for a non-isolated form of BNB compared to that of an isolated form has two characteristics: (1) high distortion energy and (2) irregular symmetry breaking (Table 4 and Figures 2 and 3). Although the total wave functions of each molecule for Φ_n^{BNB} under the permutation of electron coordinates are antisymmetric, the product states of these non-bonded molecules under intermolecular exchanges of the electrons cannot be antisymmetric. Therefore, when the two B–N bonds are asymmetrically stretched, the "$4\sigma_g^2$" and "$3\sigma_u^1$" orbitals cannot be degenerate. On the other

hand, there are major problems for introducing intermolecular antisymmetries because the antisymmetrized unperturbed states are no longer an eigenfunction of $H^{(0)}$, which follow the non-commutation of $\left[\widetilde{A},\ H^{(0)}\right] \neq 0$.

Table 3. Charges from ECP (effective core potential) fitting for BNB with several methods and basis sets.

State of BNB	BN Bonds	$\gamma=\frac{V_B-V_N}{r_{BN}}$	force $=(\Sigma_x^2+\Sigma_y^2+\Sigma_y^2)^{\frac{1}{2}}$, θ=Angle of Force Vector, $\delta(q_B-q_N)$ from ECP	$B^{\delta q_1}$–$N^{\delta q_2}$–$B^{\delta q_3}$ $\Delta=r_1(B_1N)-r_2(B_2N)$ Charges from ESP Fitting
$\widetilde{X}^2\Sigma_u^+$ Radical	B_1-N B_2-N	$\gamma=4.7201$ [a] $\gamma=4.7193$ [a]	0.89, 51.22°, 0.807 [a] 0.90, −39.11°, 0.806 [a]	$\Delta^k=0.03$ & $\delta q_1=0.23$, $\delta q_2=-0.46$, $\delta q_3=0.23$
$\widetilde{X}^1\Sigma_g^+$ Anion	B_1-N B_2-N	$\gamma=4.6213$ [a] $\gamma=4.6195$ [a]	1.09, 85.12°, 0.807 [a] 1.11, −31.15°, 0.806 [a]	$\Delta^u=0.02$ & $\delta q_1=0.10$, $\delta q_2=-0.92$, $\delta q_3=-0.18$
$\widetilde{X}^1\Sigma_g^+$ Cation	B_1-N B_2-N	$\gamma=4.5197$ [a] $\gamma=4.5199$ [a]	1.15, 75.22°, 0.807 [a] 1.19, −27.11°, 0.806 [a]	$\Delta^u=0.04$ & $\delta q_1=0.056$, $\delta q_3=-0.08$, $\delta q_2=0.52$

[a] QCISD/EPR-III; [u] m062x/6-31g*; [k] b3p86/6-31g*.

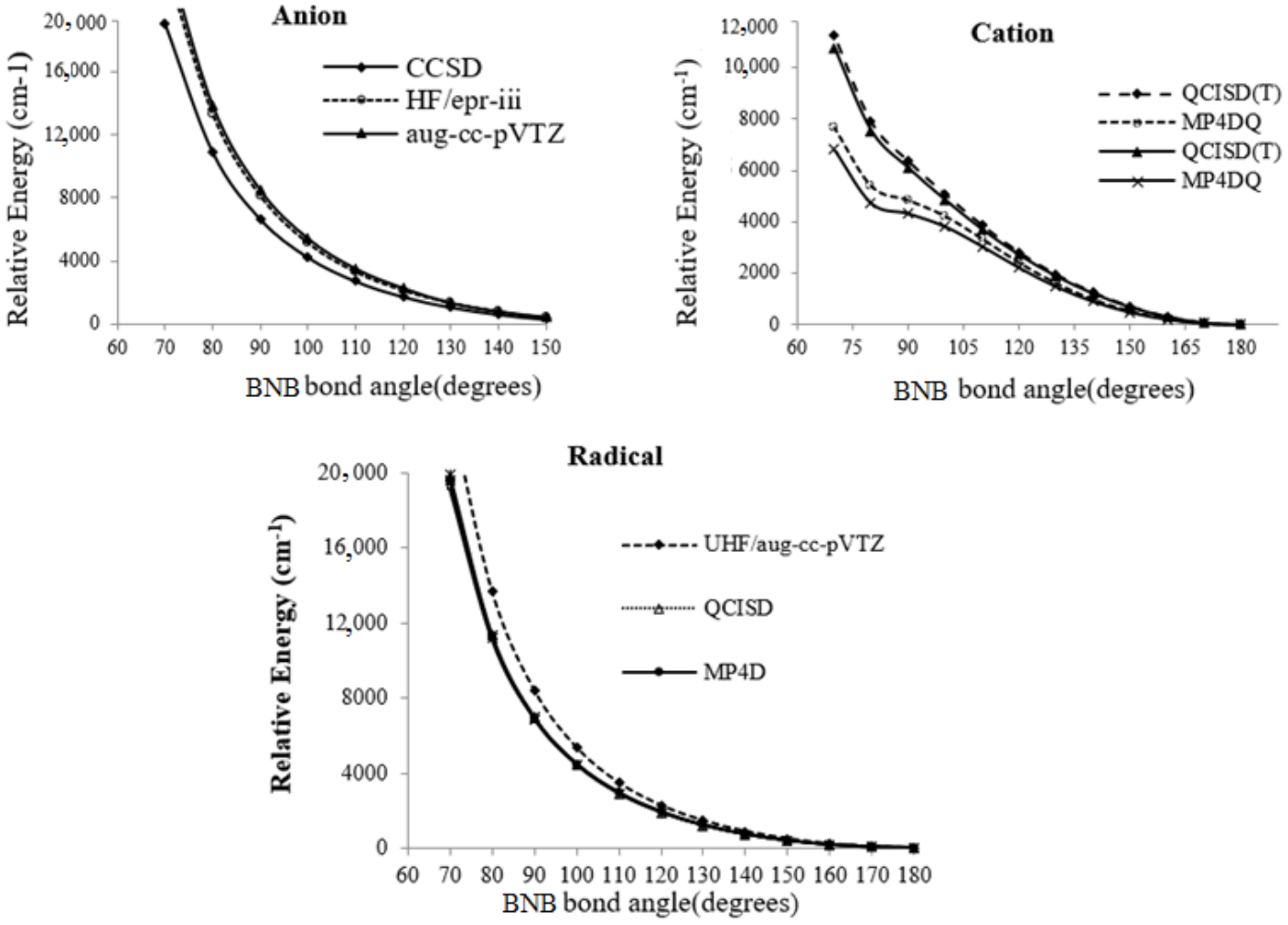

Figure 2. Relative energies of $B_2N^{(-,0,+)}$ versus B-N-B bond angle at various levels of the theory.

Table 4. The NBO, electric potential, anisotropic spin dipole couplings (ASDF), isotropic Fermi contact coupling $\{IFCC[f(\Delta)], IFCC[f(\theta)]\}$, atomic occupancies and Fock Matrix data of isolated and non-isolated forms of $B_2N^{(-,0,+)}$ in ground and excited states.

State (* N_e)	Hybrids Coefficient&	$E_{acceptor_{(j)}} - E_{Donor_{(i)}}$ ** Fock Matrix ($F_{i,j}$, *a.u.*)	Atomic Occupancies
$\widetilde{X}^1\Sigma_g^+$ (* 18e)	$\|\psi\rangle_{BD(2)} = 0.66SP_{N_1}^{1.0} + 0.75SP_{B_2}^{1.0}$ [a] $\|\psi\rangle_{BD(3)} = 0.95SP_{N_1}^{1.0} + 0.32SP_{B_2}^{1.0}$ [a] $\|\psi\rangle_{BD^*(1)} = 0.44SP_{N_1}^{1.01} - 0.90\ SP_{B_2}^{2.24}$ [a] $\|\psi\rangle_{BD^*(2)} = 0.75SP_{N_1}^{1.0} - 0.67\ SP_{B_3}^{1.0}$ [a]	$\|\psi\rangle_{BD^*(3)} - \|\psi\rangle_{BD(1)} = 1.94$ ** 0.107 $\|\psi_{BD^*(1)} - \|\psi\rangle_{BD(1)} = 0.73$ ** 0.021	$\|\alpha,\beta\rangle\ N : 2s^{1.59}2P_x^{1.70}2P_y^{1.70}2P_z^{1.66}$ $\|\alpha,\beta\rangle\ B : 2s^{0.97}2P_x^{0.14}2P_y^{0.14}2P_z^{0.37}$
$\widetilde{A}^3\Pi_u$ (* 18e)	$\|\psi\rangle_{BD(2)} = 0.97SP_{N_1}^{1.0} + 0.26SP_{B_2}^{1.0}$ [h] $\|\psi\rangle_{BD(3)} = 0.91SP_{N_1}^{1.0} + 0.40SP_{B_3}^{1.62}$ [h] $\|\psi\rangle_{BD(4)} = 0.70SP_{B_2}^{0.51} + 0.70SP_{B_3}^{0.51}$ [g] $\|\psi\rangle_{BD^*(1)} = 0.4SP_{N_1}^{1.0} - 0.91\ SP_{B_2}^{1.62}$ [h]	$\|\psi\rangle_{BD^*(3)} - \|\psi_{BD(1)} = 1.94$ ** 0.107 $\|\psi\rangle_{BD^*(4)} - \|\psi\rangle_{BD(1)} = 1.01$ ** 0.064	$\|\alpha\rangle\ N : 2s^{0.75}2P_x^{0.81}2P_y^{0.60}2P_z^{0.86}$ $\|\alpha\rangle\ B : 2s^{0.74}2P_x^{0.09}2P_y^{0.70}2P_z^{0.43}$ $\|\beta\rangle\ N : 2s^{0.80}2P_x^{0.87}2P_y^{0.90}2P_z^{0.86}$
$\widetilde{B}^3\Sigma^+$ (* 16e)	$\|\psi\rangle_{BD(1)} = 0.90SP_{N_1}^{1.0} + 0.42\ SP_B^{0.72}$ [h] $\|\psi\rangle_{BD(2)} = 0.96SP_{N_1}^{1.0} + 0.26SP_B^{1.0}$ [h] $\|\psi\rangle_{BD(3)} = 0.96SP_{N_1}^{1.0} + 0.26SP_B^{1.0}$ [f]	$\|\psi\rangle_{BD^*(3)} - \|\psi\rangle_{BD(1)} = 1.98$ ** 0.119 $\|\psi\rangle_{BD^*(1)} - \|\psi\rangle_{BD(2)} = 0.77$ ** 0.028	$\|\alpha\rangle\ N : 2s^{0.78}2P_x^{0.81}2P_y^{0.81}2P_z^{0.87}$ $\|\alpha\rangle\ B : 2s^{0.72}2P_x^{0.92}2P_y^{0.92}2P_z^{0.44}$ $\|\beta\rangle\ N : 2s^{0.77}2P_x^{0.87}2P_y^{0.87}2P_z^{0.86}$

[a] QCISD/EPR-III; [h] QCISD(T)/EPR-III; [f] b3lyp/6-31g*(pop=chelp G); [g] m062x/6-31g*(pop=chelp G). * = Number of electrons; ** = Fock Matrix ($F_{i,j}$, *a.u.*)

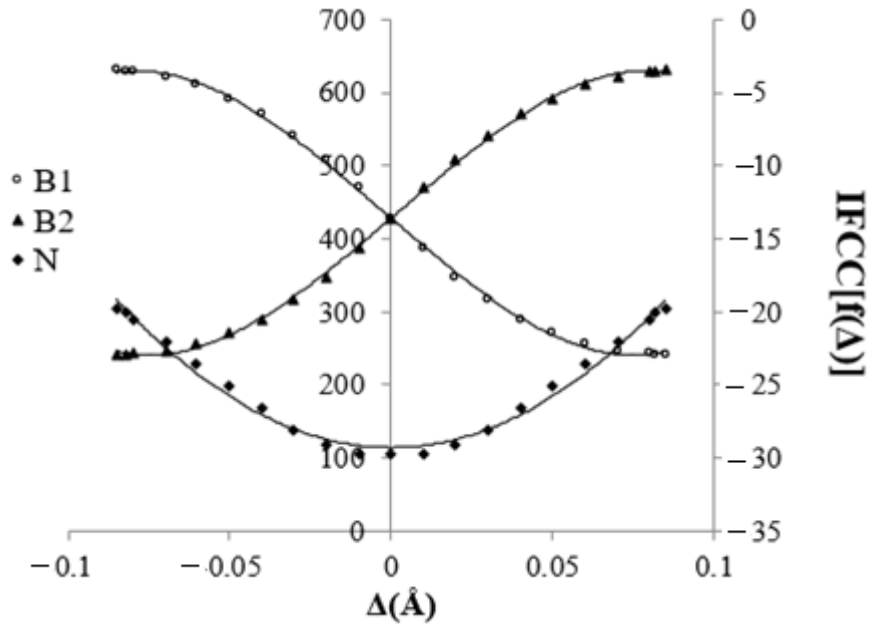

Figure 3. Isotropic Fermi contact coupling (IFCC) of $B_2N^{(0)}$.

In this study, our focus was to obtain results from DFT methods, such as b3p86, b3lyp, m062x, m06-L and m06 for the non-bonded interaction between BNB (−, 0, +) and $B_{12}N_{12}$, which are monotonous through the comparison between different situations. The m062x, m06-L and m06-HF are new methods with good correspondences in non-bonded calculations and are useful for the energies according to the distance between two fragments in a molecule with medium (∼2–5Å) and long ranges (≥5 Å).

B3LYP is unable to describe van der Waals [53,54] complexes that are bonded by medium-range interactions such as the interactions of $B_{12}N_{12}$-BNB systems. The failure of B3LYP and most of the other popular functional to correctly describe medium-range exchanges and correlation energies limits their applicability for distant non-bonded systems (our non-bonded system has a short distance). Moreover, some recent studies have shown

that inaccuracy for medium-range exchange energies lead to large systematic errors in the prediction of molecular properties [55–59]. This is due to the fact that the spin orbital energies are related to the small bending angles of A_1 and A_2, which have an extremely low bending frequency of 70 cm^{-1}.

Spin orbital energies are related to the small bending angles of A_1 and A_2, which have an extremely low bending frequency of 70 cm^{-1}. As observed in Tables 3 and 4, the results of m062x including epr-ii and 6–31 g* basis sets, compared to other functionals such as B3P86 and B3LYP, have different values (in lower level); however, in Table 2, the difference between the two positions of the global minima and local minima of the isolated BNB for both $|\alpha\rangle$ and $|\beta\rangle$ is 8.77 cm^{-1}. It is indicated in our harmonic frequencies that these were determined at the QCISD/EPR-III//prop=epr and characterized by 228.79 cm^{-1} ($\vartheta_1 = \vartheta_1'$, bending mode "$\pi_u$"), 1178.64 cm^{-1} (ϑ_2, symmetric stretching "σ_g") and 2146.42 (ϑ_3, asymmetric stretching "σ_u") [60–62]. The energy differences in Tables 4 and 5 indicate that the 2R basis sets/method, employing QRHF+ and QRHF-MOs, produces the closest result to FCI (full configuration interaction), even though it slightly underestimates SB effects. The reason for the improved performance of the QRHF+ MOs relative to the QRHF ones is the weaker MR (multi reference) character in the former case. We will thus employ QRHF+ MOs in our subsequent calculations. We also observe that, in general, CASSCF (10, 12) AUG-cc-pvqz tends to overestimate SB effects primarily due to the singly excited configuration. It is well known that in the presence of a strong MR character, CASSCF (10, 12) AUG-cc-pvqz tends to overestimate the correlation energy. Of course, the use of the ROHFSA MOs is not reliable in any case in view of a large energy gap in HF energies.

Table 5. ΔE among the BNB ground states having linear symmetric $R1 = R2 = 1.35$ Å and linear asymmetric $R1 = 1.25$, $R2 = 1.40$ Å geometries [1–5,13–16,63,64].

Basis Set and Method	Orbital	ΔE
QCISD/EPR-III	ROHFSA	7.34
TD/EPR-III//QCISD/EPR-III	ROHFSB	6.98
TD/EPR-III//QCISD/EPR-III	ROHFSA	7.12
MP_4D/EPR-II//QCISD/EPR-II	ROHFSB	5.99
QCISD/EPR-II	QRHF(+)	6.42
CASSCF(10,12)AUG-cc-pvqz	ROHFSA	4.33
CASSCF(11,12)/AUG-cc-pvqz	QRHF(−)	4.45
MP_4SDQ/EPR-II//QCISD/EPR-II	QRHF(+)	6.66
MP_4SDQ/EPR-III//QCISD/EPR-III	ROHFSB	7.45
m062x/EPR-II	ROHFSB	8.33
MP_4D/EPR-III//QCISD/EPR-III	ROHFSB	6.88
MP_4D/EPR-II//QCISD/EPR-II	ROHFSB	7.21
CBS4O	ROHFSA	7.93
CASSCF(11,12)/UHF	ROHFSB	6.83
TD/EPR-III//QCISD (T)/EPR-III	QRHF(−)	7.19
TD/EPR-II	QRHF(+)	7.55
QCISD(T)/EPR-III	ROHFSA	7.36

4. Conclusions

The results of this study made it pretty clear that the SB problem is not a real phenomenon; it is a hidden function depending on various variables such as charge distribution, bond length, IFCC, Gaussian primitives, trial wave function properties. It is indicated that the SB is generally applied to the electronic wave function failure in order to be trans-

formed as an irreducible representation of the molecular point group; thus, the failure of the electronic wave function is purely artifactual. It is not wise to conclude that only a special level of theory on the symmetry breaking for BNB is real, which is something that has been concluded in some references. Within the subject of quantum theory, the term "spatial symmetry breaking" can be interpreted in two ways: first, the lack of a broken wave function for transformations as an irreducible representation of the related point group and the second is the preference of a nuclear framework for a lower-symmetry geometry. The first item is due to the approximate wave function or artifactual in which the proper wave functions. The second item is related to the real or artifactual wave function and symmetry breaking in the nuclear framework due to the first-order Jahn–Teller effects.

Author Contributions: Conceptualization and idea, M.M.; Methodology, F.M. and M.M.; Software, F.M., M.M. and N.S.S.; Validation, M.M. and N.S.S.; Formal analysis, F.M. and M.M.; Investigation, F.M. and M.M.; Data Curation, N.S.S.; Writing—original draft preparation, M.M.; Writing—review and editing, F.M. and N.S.S.; Visualization, F.M., M.M. and N.S.S.; Supervision, M.M.; Resources, N.S.S.; Project administration, M.M. All authors have read and agreed to the published version of the manuscript.

Funding: This research received no external funding.

Data Availability Statement: The data has been mostly achieved using ab-initio calculations and some parts of them are from other works that have been cited in the right place.

Acknowledgments: The authors thank IAU University and also thank the Kastamonu University for providing library, books and scientific journals.

Conflicts of Interest: The authors declare no conflict of interest.

References

1. Martin, J.M.L.; François, J.-P.; Gijbels, R. Ab initio study of boron, nitrogen, and boron–nitrogen clusters. I. Isomers and thermochemistry of B_3, B_2N, BN_2, and N_3J. *Chem. Phys.* **1989**, *90*, 6469. [CrossRef]
2. Asmis, K.R.; Taylor, T.R.; Neumark, D.M. Anion photoelectron spectroscopy of $B2N^-$. *J. Chem. Phys.* **1999**, *111*, 8838. [CrossRef]
3. Martin, J.M.L.; François, J.-P.; Gijbels, R. Some cost-effective approximations to CCSD and QCISD. *Chem. Phys. Lett.* **1990**, *172*, 354–360. [CrossRef]
4. Knight, L.B.; Hill, D.W., Jr.; Kirk, T.J.; Arrington, C.A. Laser vaporization generation of $B^{14}NH$, $B^{15}NH$, $B^{14}ND$, $B^{16}O$, and $B^{17}O$: Electron-spin-resonance investigation in neon matrices under ultracold trapping conditions. *J. Phys. Chem.* **1992**, *96*, 5604. [CrossRef]
5. Martin, J.M.L.; François, J.-P.; Gijbels, R. The structure, stability, and infrared spectrum of B_2N, B_2N^+, B_2N^-, BO, B_2O and B_2N_2. *Chem. Phys. Lett.* **1992**, *193*, 243–250. [CrossRef]
6. Hassanzadeh, P.; Andrews, L. Pulsed laser-assisted reactions of boron and nitrogen atoms in a condensing nitrogen stream. *J. Phys. Chem.* **1992**, *96*, 9177–9182. [CrossRef]
7. Andrews, L.; Hassanzadeh, P.; Burkholder, T.R.; Martin, J.M.L. Reactions of pulsed laser produced boron and nitrogen atoms in a condensing argon stream. *J. Chem. Phys.* **1993**, *98*, 922. [CrossRef]
8. Thompson, C.A.; Andrews, L. Reactions of B Atoms with NH_3 to Produce HBNH, BNBH, and B_2N. *J. Am. Chem. Soc.* **1995**, *117*, 10125–10126. [CrossRef]
9. Li, X.; Paldus, J. Real or artifactual symmetry breaking in the BNB radical: A multireference coupled cluster viewpoint. *J. Chem. Phys.* **2007**, *126*, 224304. [CrossRef]
10. Martin, J.M.L.; El-Yazal, J.; François, J.-P.; Gijbels, R. The structure and energetics of B_3N_2, B_2N_3, and BN_4. *Mol. Phys.* **1995**, *85*, 527–537. [CrossRef]
11. Meloni, G.; Sai Baba, M.; Gingerich, A. Knudsen cell mass spectrometric investigation of the B_2N molecule. *J. Chem. Phys.* **2000**, *113*, 8995. [CrossRef]
12. Graham, W.R.M.; Weltner, W., Jr. B atoms, B_2 and H_2BO molecules: ESR and optical spectra at 4 °K. *J. Chem. Phys.* **1976**, *65*, 1516–1521. [CrossRef]
13. Monajjemi, M. Non bonded interaction between BnNn (stator) and $BN^{(-,0,+)}B$ (rotor) systems: A quantum rotation in IR region. *Chem. Phys.* **2013**, *425*, 29–45. [CrossRef]
14. Monajjemi, M.; Lee, V.S.; Khaleghian, M.; Honarparvar, B.; Mollaamin, F. Theoretical Description of Electromagnetic Nonbonded Interactions of Radical, Cationic, and Anionic $NH_2BHNBHNH_2$ Inside of the $B_{18}N_{18}$ Nanoring. *J. Phys. Chem. C* **2010**, *114*, 15315–15330. [CrossRef]
15. Monajjemi, M.; Boggs, J.E. A New Generation of BnNn Rings as a Supplement to Boron Nitride Tubes and Cages. *J. Phys. Chem. A* **2013**, *117*, 1670–1684. [CrossRef] [PubMed]

16. Monajjemi, M. Quantum investigation of non-bonded interaction between the $B_{15}N_{15}$ ring and BH_2NBH_2 (radical, cation, anion) systems: A nano molecularmotor. *Struct. Chem.* **2012**, *23*, 551–580. [CrossRef]
17. Walsh, A.D. The electronic orbitals, shapes, and spectra of polyatomic molecules. Part I. AH_2 molecules. *J. Chem. Soc.* **1953**, 2260–2266. [CrossRef]
18. Wigner, E.P. *Group Theory and Its Application to the Quantum Mechanics of Atomic Spectra*; Academic Press: New York, NY, USA, 1959; p. 259.
19. Löwdin, P.O. Proton tunneling in DNA and its biological implications. *Rev. Mod. Phys.* **1963**, *35*, 496. [CrossRef]
20. Barone, V. *Recent Advances in Density Functional Methods*; Parts, I., Chong, D.P., Eds.; World Scientific Publishing Co., Springer: Berlin/Heidelberg, Germany, 1996.
21. Chopra, N.G.; Luyken, R.J.; Herrey, K.; Crespi, V.H.; Cohen, M.L.; Louie, S.G.; Zettl, A. Boron Nitride Nanotubes. *Science* **1995**, *269*, 966–967. [CrossRef]
22. Blase, X.; Rubio, A.; Louie, S.G.; Cohen, M.L. Stability and Band Gap Constancy of Boron Nitride Nanotubes. *Europhys. Lett. (EPL)* **1994**, *28*, 335–340. [CrossRef]
23. Blase, X.; Charlier, J.C.; de Vita, A.; Car, R. Theory of composite B*x*C*y*N*z* nanotube heterojunctions. *Appl. Phys. Lett.* **1997**, *70*, 197. [CrossRef]
24. Han, W.; Bando, Y.; Kurashima, K.; Sato, T. Synthesis of boron nitride nanotubes from carbon nanotubes by a substitution reaction. *Appl. Phys. Lett.* **1998**, *73*, 3085. [CrossRef]
25. Walker, T.E.H.; Richards, W.G. Molecular spin-orbit coupling constants. Role of core polarization. *J. Chem. Phys.* **1970**, *52*, 1311. [CrossRef]
26. Koseki, S.; Schmidt, M.W.; Gordon, M.S. MCSCF/6-31G(d,p) calculations of one-electron spin-orbit coupling constants in diatomic molecules. *J. Phys. Chem.* **1992**, *96*, 10768–10772. [CrossRef]
27. Pople, J.A.; Head-Gordon, M.; Raghavachari, K. Quadratic configuration interaction. A general technique for determining electron correlation energies. *J. Chem. Phys.* **1987**, *87*, 5968. [CrossRef]
28. Bader, R.F.W. *Atoms in Molecule: A Quantum Theory*; Oxford University Press: Oxford, UK, 1990.
29. Besler, B.H.; Merz, K.M., Jr.; Kollman, P.A. Atomic Charges Derived from Semiempirical Methods. *J. Comput. Chem.* **1990**, *11*, 431–439. [CrossRef]
30. Chirlian, L.E.; Francl, M.M. Atomic Charges Derived from Electrostatic Potentials: A Detailed Study. *J. Comput. Chem.* **1987**, *8*, 894–905. [CrossRef]
31. Breneman, C.M.; Wiberg, K.B. Determining Atom-Centered Monopoles from Molecular Electrostatic Potentials. The Need for High Sampling Density in Formamide Conformational Analysis. *J. Comput. Chem.* **1990**, *11*, 361–373. [CrossRef]
32. Najaflou, N.; Monajjemi, M. A NMR Study of Sodium/Potassium Pumping System in the Node of Ranvier Myelin-Sheath. *Biointerface Res. Appl. Chem.* **2021**, *11*, 14260–14277. [CrossRef]
33. Monajjemi, M.; Kandemirli, F.; Sakhaeinia, H.; Mollaamin, F. Biophysical Interface of Anti-Matter for Virtual Living in Real World: A Reality in Chemical Converted in Parallel Worlds. *Biointerface Res. Appl. Chem.* **2022**, *12*, 2646–2659. [CrossRef]
34. Martin, F.; Zipse, H. Charge distribution in the water molecule—A comparison of methods. *J. Comput. Chem.* **2005**, *26*, 97–105. [CrossRef] [PubMed]
35. Frisch, M.J.; Trucks, G.W.; Schlegel, H.B.; Scuseria, G.E.; Robb, M.A.; Cheeseman, J.R.; Scalmani, G.; Barone, V.; Mennucci, B.; Petersson, G.A.; et al. *Gaussian 09*; Gaussian Inc.: Wallingford, CT, USA; Oxfordshire, UK, 2009.
36. Monajjemi, M.; Mahdavian, L.; Mollaamin, F.; Khaleghian, M. Interaction of Na, Mg, Al, Si with carbon nanotube (CNT): NMR and IR study. *Russ. J. Inorg. Chem.* **2009**, *54*, 1465–1473. [CrossRef]
37. Bakhshi, K.; Mollaamin, F.; Monajjemi, M. Exchange and correlation effect of hydrogen chemisorption on nano V(100) surface: A DFT study by generalized gradient approximation (GGA). *J. Comput. Theor. Nanosci.* **2011**, *8*, 763–768. [CrossRef]
38. Tahan, A.; Mollaamin, F.; Monajjemi, M. Thermochemistry and NBO analysis of peptide bond: Investigation of basis sets and binding energy. *Russ. J. Phys. Chem. A* **2009**, *83*, 587–597. [CrossRef]
39. Mollaamin, F.; Monajjemi, M. Harmonic Linear Combination and Normal Mode Analysis of Semiconductor Nanotubes Vibrations. *J. Comput. Theor. Nanosci.* **2015**, *12*, 1030–1039. [CrossRef]
40. Monajjemi, M. Cell membrane causes the lipid bilayers to behave as variable capacitors: A resonance with self-induction of helical proteins. *Biophys. Chem.* **2015**, *207*, 114–127. [CrossRef]
41. Monajjemi, M. Liquid-phase exfoliation (LPE) of graphite towards graphene: An ab initio study. *J. Mol. Liq.* **2017**, *230*, 461–472. [CrossRef]
42. Monajjemi, M.; Bagheri, S.; Moosavi, M.S.; Moradiyeh, N.; Zakeri, M.; Attarikhasraghi, N.; Saghayimarouf, N.; Niyatzadeh, G.; Shekarkhand, M.; Khalilimofrad, M.S.; et al. Symmetry breaking of $B_2N^{(-,0,+)}$: An aspect of the electric potential and atomic charges. *Molecules* **2015**, *20*, 21636–21657. [CrossRef]
43. Monajjemi, M.; Mohammadian, N.T. S-NICS: An aromaticity criterion for nano molecules. *J. Comput. Theor. Nanosci.* **2015**, *12*, 4895–4914. [CrossRef]
44. Monajjemi, M.; Mollaamin, F. Ellipticity, PDI and FLU, Evaluation of Aromaticity Indexes During Substituting B &N Atoms in Poly-Annulene. *Biointerface Res. Appl. Chem.* **2021**, *11*, 8298–8317. [CrossRef]

45. Otadi, M.; Panahi Shayegh, Z.; Monajjemi, M. Synthesis and Characterization of Mn doped ZnO Nanoparticles and Degradation of Pyridine in a Batch Reactor Using: Taguchi Experimental Designing & Molecular Mechanic Simulation. *Biointerface Res. Appl. Chem.* **2021**, *11*, 12471–12482. [CrossRef]
46. Mohammad Gholiha, H.; Ghadami, A.; Monajjemi, M.; Ehsani, M. Enhanced Physical and Mechanical Properties of Flake–Shape/Vinyl-ester Nanocomposites Through Surface Modification of Graphene and Glass Flake: A Comparison with Simulated Data. *Biointerface Res. Appl. Chem.* **2021**, *11*, 11316–11337.
47. Monajjemi, M.; Robert, W.J.; Boggs, J.E. NMR contour maps as a new parameter of carboxyl's OH groups in amino acids recognition: A reason of tRNA–amino acid conjugation. *Chem. Phys.* **2014**, *433*, 1–11. [CrossRef]
48. Bagheri, S.; Monajjemi, M. A Novel Cathodic Combination in Sodium-Ion Battery Based on $NaNi_{0.7}Co_{0.3}O_2$, Na_2MnO_3, and $NaCoO_2$ Combination: Synthesis and Characterization. *Biointerface Res. Appl. Chem.* **2021**, *11*, 11316–11337.
49. Monajjemi, M. Metal-doped graphene layers composed with boron nitride–graphene as an insulator: A nanocapacitor. *J. Mol. Modeling* **2014**, *20*, 2507. [CrossRef] [PubMed]
50. Monajjemi, M.; Najafpour, J.; Mollaamin, F. $(3,3)_4$ Armchair carbon nanotube in connection with PNP and NPN junctions: Ab Initio and DFT-based studies. *Fuller. Nanotub. Carbon Nanostruct.* **2013**, *21*, 213–232. [CrossRef]
51. Monajjemi, M.; Jafari Azan, M.; Mollaamin, F. Density functional theory study on $B_{30}N_{20}$ nanocage in structural properties and thermochemical outlook. *Fuller. Nanotub. Carbon Nanostruct.* **2013**, *21*, 503–515. [CrossRef]
52. Monajjemi, M.; Baie, M.T.; Mollaamin, F. Interaction between threonine and cadmium cation in [Cd(Thr)] (n = 1–3) complexes: Density functional calculations. *Russ. Chem. Bull.* **2010**, *59*, 886–889. [CrossRef]
53. Zhao, Y.; Truhlar, D.G. Density Functionals with Broad Applicability in Chemistry. *Acc. Chem. Res.* **2008**, *41*, 157–167. [CrossRef]
54. Check, C.E.; Gilbert, T.M. Progressive Systematic Underestimation of Reaction Energies by the B3LYP Model as the Number of C−C Bonds Increases: Why Organic Chemists Should Use Multiple DFT Models for Calculations Involving Polycarbon Hydrocarbons. *J. Org. Chem.* **2005**, *70*, 9828–9834. [CrossRef]
55. Grimme, S. Seemingly Simple Stereoelectronic Effects in Alkane Isomers and the Implications for Kohn–Sham Density Functional Theory. *Angew. Chem. Int. Ed.* **2006**, *45*, 4460–4464. [CrossRef] [PubMed]
56. Wodrich, M.D.; Corminboeuf, C.; Schleyer, P.V.R. Systematic Errors in Computed Alkane Energies Using B3LYP and Other Popular DFT Functionals. *Org. Lett.* **2006**, *8*, 3631–3634. [CrossRef] [PubMed]
57. Schreiner, P.R.; Fokin, A.A.; Pascal, R.A., Jr.; de Meijere, A. Many density functional theory approaches fail to give reliable large hydrocarbon isomer energy differences. *Org. Lett.* **2006**, *8*, 3635–3638. [CrossRef] [PubMed]
58. Zhao, Y.; Truhlar, D.G. A Density Functional That Accounts for Medium-Range Correlation Energies in Organic Chemistry. *Org. Lett.* **2006**, *8*, 5753–5755. [CrossRef] [PubMed]
59. Gwaltney, S.R.; Head-Gordon, M. Calculating the equilibrium structure of the BNB molecule: Real *s*. artifactual symmetry breaking. *Phys. Chem. Chem. Phys.* **2001**, *3*, 4495–4500. [CrossRef]
60. Ding, H.; Morse, M.D.; Apetrei, C.; Chacaga, L.; Maier, J.P. Resonant two-photon ionization spectroscopy of BNB. *J. Chem. Phys.* **2006**, *125*, 194315. [CrossRef]
61. Liu, Y.; Zou, W.; Bersuker, I.B.; Boggs, J.E. Symmetry breaking in the ground state of BNB: A high level multireference study. *J. Chem. Phys.* **2009**, *130*, 184305. [CrossRef]
62. Al-Saidi, W.A. Ground state structure of BNB using fixed-node diffusion Monte Carlo. *Chem. Phys. Lett.* **2012**, *543*, 41–44. [CrossRef]
63. Kalemos, A. Symmetry breaking in a nutshell: The odyssey of a pseudo problem in molecular physics. *J. Chem. Phys.* **2013**, *138*, 224302. [CrossRef]
64. Kalemos, A.; Dunning, T.H.; Mavridis, A. On symmetry breaking in BNB: Real or artifactual? *J. Chem. Phys.* **2004**, *120*, 4. [CrossRef]